Available online at www.sciencedirect.com
ScienceDirect
Trans. Nonferrous Met. Soc. China 35(2025) 2586−2597
Transactions of Nonferrous Metals Society of China
www.tnmsc.cn

Homogenization forging and deformation mechanism of near-β titanium alloy in $\alpha+\beta$ region

Yang-zhi-hong XIAO[1], Ye-chen DENG[1], Yi-xin AN[1,2], Xiao-dong ZHAN[1], Xiao-yong ZHANG[2], Bing-feng WANG[1,2]

1. School of Materials Science and Engineering, Central South University, Changsha 410083, China;
2. State Key Laboratory of Powder Metallurgy, Central South University, Changsha 410083, China

Received 6 November 2023; accepted 26 June 2024

Abstract: The microstructures of a Ti−5Al−5Mo−5V−1Cr−1Fe alloy with a strain gradient from 0.1 to 1 were obtained by double-cone compression experiments. The deformation microstructures were analyzed by EBSD and TEM. The results show that the deformation mechanism is dynamic recovery when the strain is less than 0.42. In the strain range of 0.42−0.88, the deformation mechanism is dynamic recrystallization. When the strain exceeds 0.88, the deformation bands appear. The deformation mechanism map combined with the homogenization degree of the microstructure was constructed. The more homogeneous deformed microstructure was obtained at the strain of 0.6 and the temperature of 860 °C. The dynamic recrystallization forms new grains and reduces the size difference between the grains, which improves the homogenization degree of the microstructure.

Key words: near-β titanium alloy; hot deformation mechanism; dynamic recrystallization; homogenization degree; double-cone compression experiment

1 Introduction

Ti−5Al−5Mo−5V−1Cr−1Fe titanium alloy is a typical near-β titanium alloy and has α and β dual phases at room temperature [1]. Due to a series of advantages such as high specific strength, excellent corrosion resistance, and superior hardenability, the Ti−5Al−5Mo−5V−1Cr−1Fe titanium alloy has been applied to bearing structural parts such as aircraft fuselages and landing gear [2,3]. These structural parts are mainly formed by the forging process [4,5].

The homogeneous forging microstructure has excellent formability, which is beneficial to the subsequent processing. GUPTA et al [6] studied the forging microstructure of a Ti−6Al−2Sn−4Zr−6Mo titanium alloy and measured the fatigue properties of the microstructure with different homogenization degrees. It was demonstrated that the non-uniform deformation was unfavorable to the fatigue life. LI et al [7] found that homogeneous multiaxial forging microstructures had better high-temperature plasticity. ZHANG et al [8] found that homogeneous forging microstructures had better plasticity and fracture toughness at room temperature. The more homogeneous the deformation microstructure after forging, the better the plasticity and fracture toughness [9,10]. In the hot deformation of titanium alloy, there are many deformation mechanisms such as dynamic recovery (DRV) [11], dynamic recrystallization (DRX) [12], and deformation bands (DBs) [13] under different deformation conditions. In the study of the homogenization of deformation microstructure, it is necessary to consider the influence of different deformation conditions on the microstructure. This means that a lot of experiments need to be done, and efficient

Corresponding author: Bing-feng WANG, Tel: +86-731-88876244, E-mail: wangbingfeng@csu.edu.cn
https://doi.org/10.1016/S1003-6326(25)66834-8

experimental methods can accelerate the process.

The double-cone compression experiment is an efficient experimental technology. Compared with the cylinder compression experiment, it can achieve a continuous strain gradient in the single double-cone specimen. This means that the deformation microstructure with different strains can be quickly obtained at the same time. Many researchers carried out the double-cone compression experiment to improve the efficiency of experiments. KIM et al [14] studied the dynamic globularization of the Ti−6Al−4V titanium alloy through the double-cone compression experiment. AN et al [15] obtained the microstructure of the Ti−2.5Zr−2Al titanium alloy in the strain range of 0.2−1.2 by the double-cone compression experiment and constructed the hot deformation mechanism diagram. DENG et al [16] constructed the hot deformation mechanism diagram of a Ti−5Al−5Mo−5V−1Cr−1Fe titanium alloy by the double-cone compression experiment and studied its deformation instability. Although the single double-cone specimen can quickly obtain the microstructures with gradient strain, it cannot directly obtain the strain of each region on the specimens. In order to solve this trouble, finite element simulation is often used to obtain the strain distribution of the double-cone specimens.

In the present work, the microstructure with the strain range of 0.1−1 was obtained by the double-cone compression experiment. The deformation mechanism of the Ti−5Al−5Mo−5V−1Cr−1Fe titanium alloy was analyzed by EBSD and TEM. The homogenization degree of the microstructure was characterized according to the grain size and shape. The homogenization degree and deformation mechanism of the microstructure under different deformation conditions were analyzed.

2 Experimental

The chemical compositions of the Ti−5Al−5Mo−5V−1Cr−1Fe titanium alloy are shown in Table 1. The initial microstructure of the Ti−5Al−5Mo−5V−1Cr−1Fe titanium alloy is an equiaxed structure, as shown in Fig. 1, which is composed of the β phase and the equiaxial α phase.

Figure 2(a) shows the geometric model of the double-cone specimens. The double-cone specimens were heated by a resistive heating furnace in vacuum to 850, 870, and 890 °C, respectively. They were kept at the deformation temperature for 900 s. The specimens were compressed using a hydraulic press at a strain rate of 1 s^{-1} and a height decrease of 10 mm. The specimens were quenched in water after the hot compression. The hot deformation process was simulated by the finite element software Deform-3D. Several areas of the specimens can be identified as edge, middle, and center.

Table 1 Chemical compositions of Ti−5Al−5Mo−5V−1Cr−1Fe titanium alloy (wt.%)

Al	Mo	V	Cr	Fe	Ti
5.16	4.92	4.96	1.10	0.98	Bal.

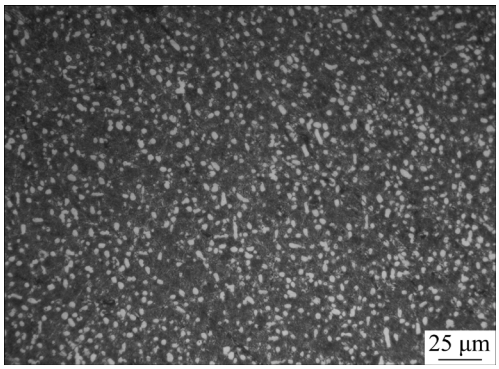

Fig. 1 Initial microstructure of Ti−5Al−5Mo−5V−1Cr−1Fe titanium alloy

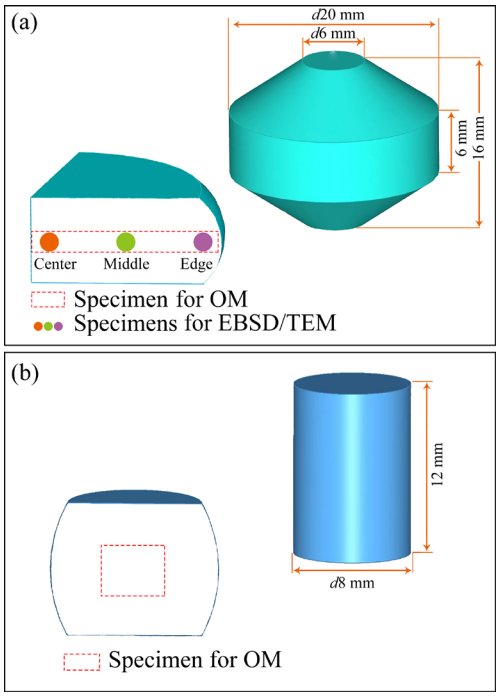

Fig. 2 Geometric models and sampling positions of double-cone specimens (a) and cylinder specimens (b)

There are cylinder specimens for the thermal simulation compression experiment. Figure 2(b) shows the size of the cylinder specimens. The heating and compression processes of the specimens were completed on a Gleeble 3180 thermal simulator. Before the hot compression, the cylinder specimens were respectively heated to 860, 870, and 880 °C under vacuum conditions with a heating rate of 10 °C/s. The true strains of the three specimens are 0.5, 0.6, and 0.7 at each temperature. Then, they were kept at the deformation temperature for 300 s to ensure that the overall temperature was consistent. The specimens were quenched in water after the hot compression.

All deformed specimens were cut from the center along the compression direction and polished. The metallographic etching solution is made up of 92 vol.% water, 2 vol.% hydrofluoric acid, and 6 vol.% nitric acid. The POLYVAR-MET metallographic microscope (Leica, Germany) was used to characterize the metallographs. The grain size was measured by the Image-Pro Plus 6.0 software.

The foils from different areas of the double-cone specimens were cut to a thickness of 0.5 mm along the loading axis by wire cutting. The foils were ground and polished to a thickness less than 80 μm and disks with a diameter of 3 mm were punched out of these thin foils. The disks were prepared by the double-jet electrochemical method at a voltage of 27 V, a temperature of −30 °C, and a working time of 100 s. The composition of the double-jet electrolyte was 50 mL of perchloric acid, 350 mL of normal butanol, and 600 mL of methanol.

The foils from different areas of the double-cone specimens were used for EBSD observations. The EVOMA10 (ZEISS, Germany) scanning electron microscope was used to collect the EBSD data. The OIM Analysis (EDAX, America) software was used to analyze the EBSD data. The grain boundaries in solid black lines denote the HAGBs with angles larger than 15°, and the grain boundaries in thin white lines represent the LAGBs with angles larger than 2° and smaller than 15° in the inverse pole figure (IPF).

The foils from the middle of the double-cone specimens were used for TEM observations. The Tecnai G2 20ST (FEI, Netherlands) transmission electron microscope was used to capture the TEM images.

3 Results

3.1 Double-cone compression experimental results

The metallographs of the double-cone specimens and the simulation results are shown in Fig. 3. The distribution of true strain was analyzed using the finite element method. The relevant parameters of the simulation method are shown in Section A in Supplementary Materials. The post-processing module of the DEFORM software was used to analyze the deformed double-cone specimen. The longitudinal section was selected to analyze the distribution of strain, as shown in Fig. 2(a). The distribution of strain was matched with the position of metallographic analysis, as shown in Fig. 3. In the metallographical montages, coarse grains can be observed in the edge area. With the increase of true strain, the grains gradually

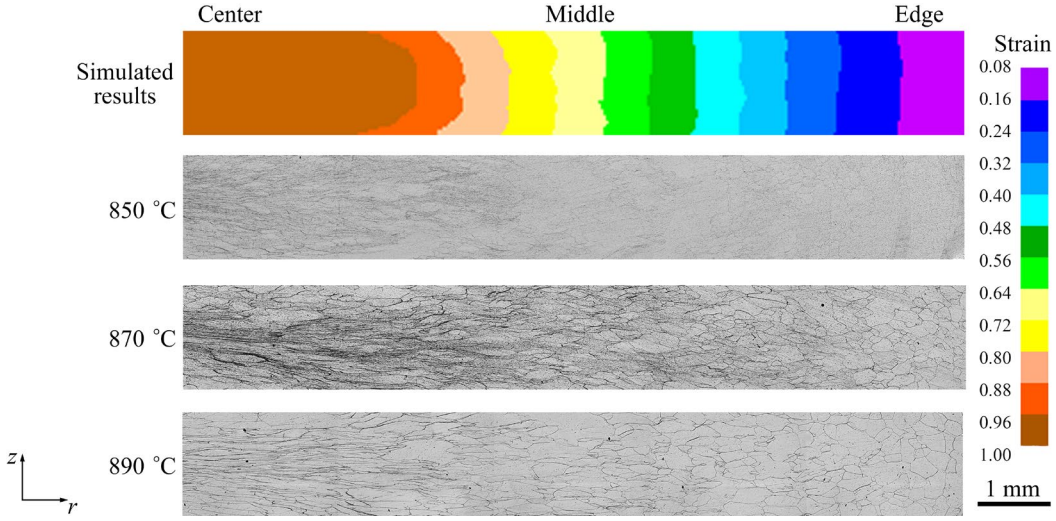

Fig. 3 Metallographs of double-cone specimens and corresponding simulation results by finite element method

become finer. When the true strain exceeds 0.88, DBs appear, which represents the occurrence of deformation instability. Therefore, the strains higher than 0.88 should be avoided in the process of hot deformation.

In order to express the homogenization degree of the microstructure, the dispersion coefficient (D) and homogenization index (H) are introduced. The dispersion coefficient D is defined as follows [17]:

$$D=\frac{S}{E}\times 100\% \tag{1}$$

where E and S represent the average value and the standard deviation of the grain size, respectively. The higher the D value, the higher the dispersion degree.

In order to comprehensively consider the dispersion degree of grain size and shape, the concept of homogenization index is proposed to represent the homogenization degree of microstructure. The homogenization index H is defined as follows [18]:

$$H=(1-D_z)(1-D_r)(1-D_S) \tag{2}$$

where D_z represents the dispersion coefficient of grain size along the z-axis, D_r represents the dispersion coefficient of grain size along the r-axis, and D_S represents the dispersion coefficient of the shape factor of the grain. The shape factor (S_1) is defined as follows [15]:

$$S_1=d_z/d_r \tag{3}$$

where d_r and d_z represent the grain sizes along the r-axis and z-axis, respectively. The grain sizes along different directions were measured by the linear intercept method. The directions of the z-axis and r-axis are shown in Fig. 3. The average values of the linear intercept length are used to represent the grain size along these directions. The larger the homogenization index, the higher the homogenization degree of the microstructure.

Figure 4 shows the dispersion coefficient D and homogenization index H of the microstructure with different true strains in the double-cone specimens. In Fig. 4(d), the homogenization index reaches a maximum of 0.63 under the strain of 0.6 at 870 °C. In this work, the microstructure with an

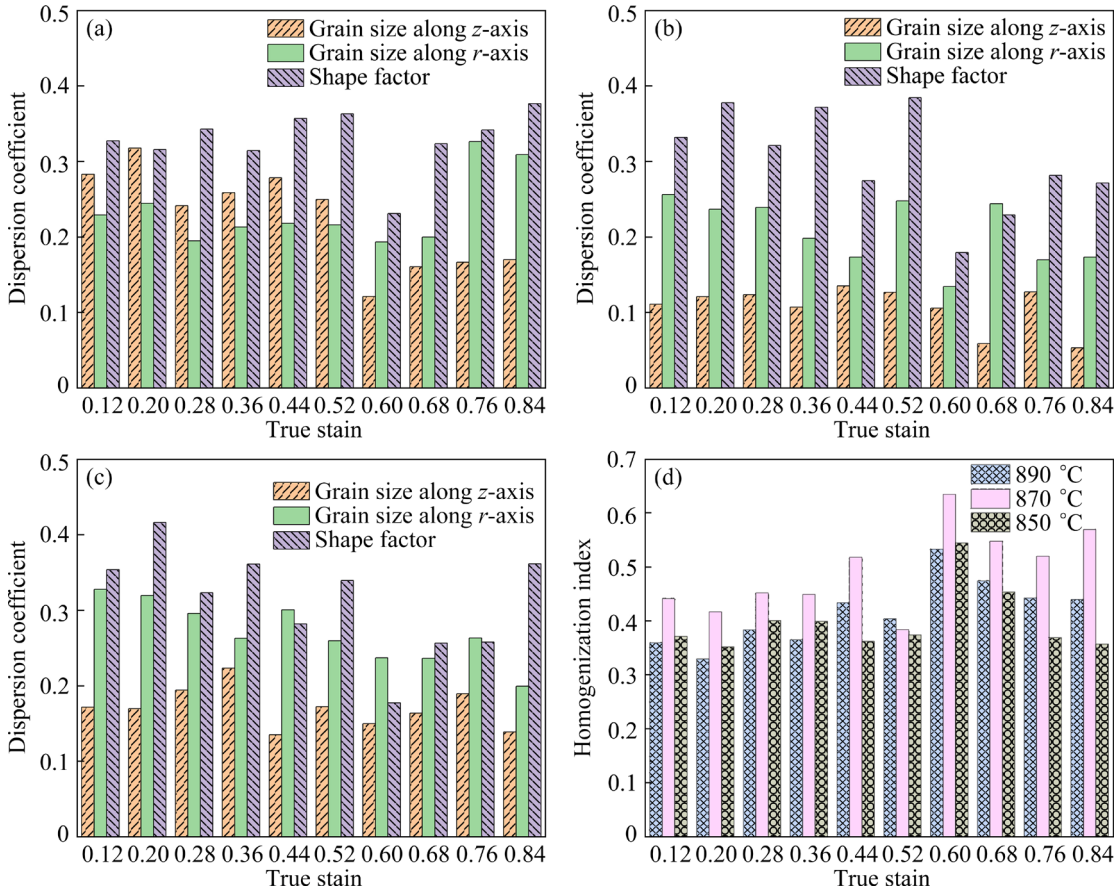

Fig. 4 Dispersion coefficient (a−c) and homogenization index (d) of microstructure with different true strains in double-cone specimens

H value higher than 0.6 is considered to be homogeneous. The temperature of 870 °C and the strain of 0.6 are considered to be reasonable deformation conditions for the double-cone compression experiment. Therefore, the cylinder compression tests in the strain range of 0.5−0.7 and the temperature range of 860−880 °C were carried out to verify this result.

3.2 Cylinder compression experimental results

Figure 5 shows the comparative results of the double-cone and cylinder specimens. Figure 5(a) shows the average grain sizes under different true strains in the double-cone and cylinder specimens. The curves are drawn according to the grain size data from the double-cone specimens, and the orange dots are drawn according to the grain size data from the cylinder specimens. Under the same strain, the deformation microstructure in the double-cone specimens has an average grain size that is identical to that of the cylinder specimens. The metallograph for the double-cone specimen in the strain range of 0.48−0.56 at 870 °C is shown in Fig. 5(b). The metallograph in the cylinder specimen is shown in Fig. 5(c). The grain shape of the deformation microstructure in the cylinder specimen is similar to that in the double-cone specimen under the same true strain.

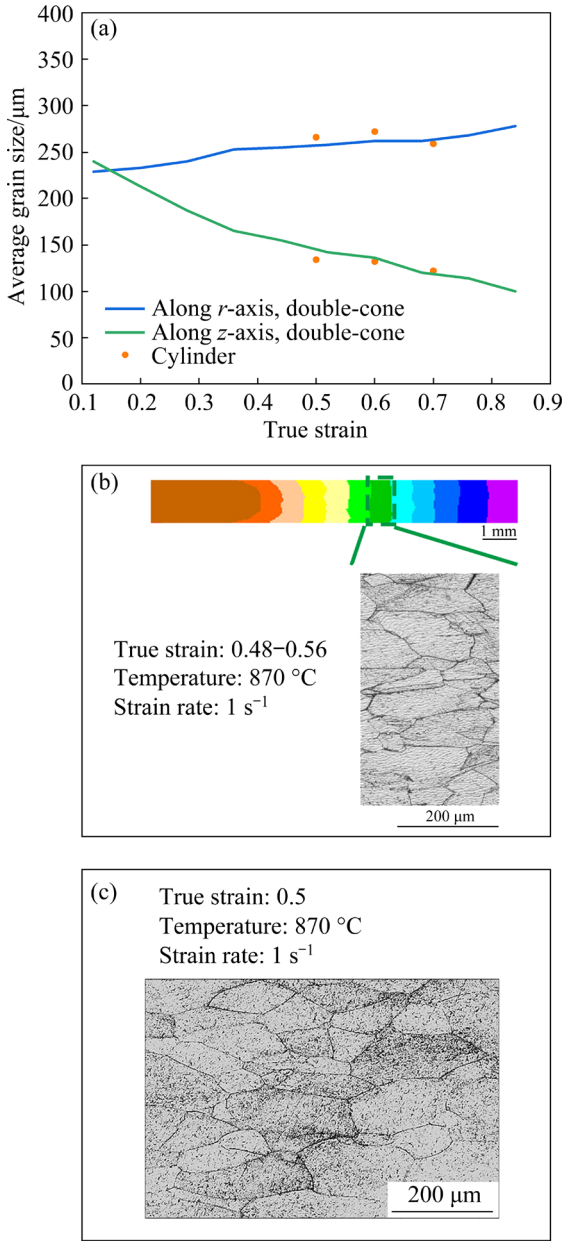

Fig. 5 Comparative results of double-cone and cylinder specimens: (a) Average grain size; (b, c) Metallographs in double-cone and cylinder specimens, respectively

Whether from the perspective of grain size or grain shape, the double-cone specimen with the same true strain has a similar deformation microstructure to the cylinder specimen. This means that the microstructure of the cylinder specimen can be represented by the microstructure of the double-cone specimen in the same strain region.

Figure 6 shows the statistical results of homogenization degree in the cylinder specimens. The homogenization indexes in the strain range of 0.5−0.7 and the temperature range of 860−880 °C are shown in Fig. 6(a). The homogenization index reaches a maximum of 0.66 under the strain of 0.6 at 860 °C. The homogenization index in the double-cone specimens reaches a maximum of 0.63 under the strain of 0.6 at 870 °C. The strain in this result is identical to the strain in the result in the cylinder compression experiment. Figure 6(b) shows the homogenization index of the deformed microstructure under the strain of 0.6 and different temperatures. When the temperature is 860 °C, the homogenization index of the deformed microstructure is the highest. This means that the deformation microstructure is more homogeneous under the strain of 0.6 at 860 °C in the cylinder specimens. The microstructure under this deformation condition is shown in Fig. 6(c).

3.3 Microstructure

The IPFs for various areas in the double-cone specimen are shown in Fig. 7. There are several coarse grains and some LAGB in the edge area, as seen in Fig. 7(a). Because of the slight strain in the edge area, the level of the DRV is low [19]. In Fig. 7(b),

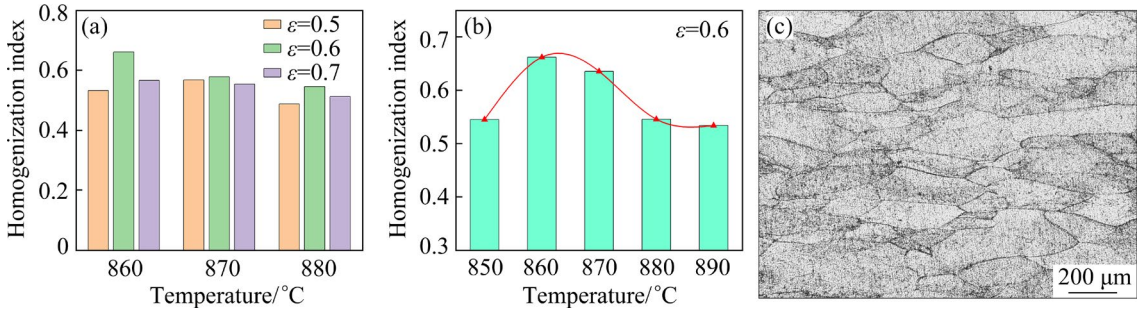

Fig. 6 Homogenization index of cylinder specimens under different conditions (a, b), and metallograph of cylinder specimen deformed under strain of 0.6 at 860 °C (c)

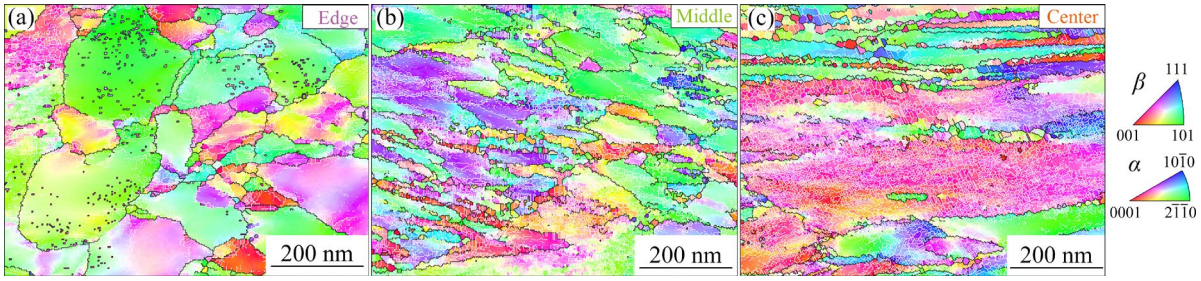

Fig. 7 IPFs at edge (a), middle (b), and center (c) of double-cone specimen deformed at 870 °C

the grains become fine and the polygonal fine grains appear in the middle area. This means that the DRX took place under this deformation condition [20]. In Fig. 7(c), the serrated grain boundaries surrounded by some fine grains can be observed in the center area.

Figure 8 shows the EBSD analysis results of the middle area in the double-cone specimen deformed at 870 °C. The IPF of the microstructure is shown in Fig. 8(a). There is a line *AB* that passes through five subgrains. Figure 8(b) shows the misorientation line chart from Position *A* to Position *B*. In the misorientation line chart, it is clear that the point-to-origin misorientation is over 25°. This indicates that there is a misorientation between two positions in the grain exceeding 25°. This means that there is subgrain lattice rotation in this grain [21,22]. The characteristic of continuous dynamic recrystallization (CDRX) is the obvious gradient of misorientation in the initial grain [23]. Therefore, the main deformation mechanism is CDRX in this deformation condition.

Figure 9 shows the TEM images of the middle area in the double-cone specimens deformed at 870 °C. Figure 9(a) shows the dislocation tangle occurred in the deformed grain. Figure 9(b) shows the polygonal subgrain surrounded by dislocations. Figure 9(c) shows the subgrain coalescence occurred

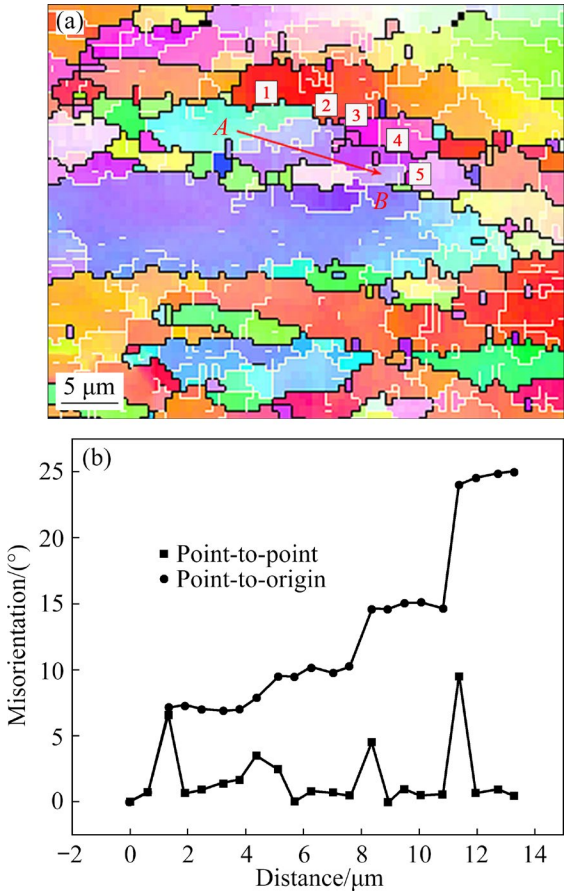

Fig. 8 EBSD results of middle area in double-cone specimens deformed at 870 °C: (a) IPF; (b) Misorientation line chart

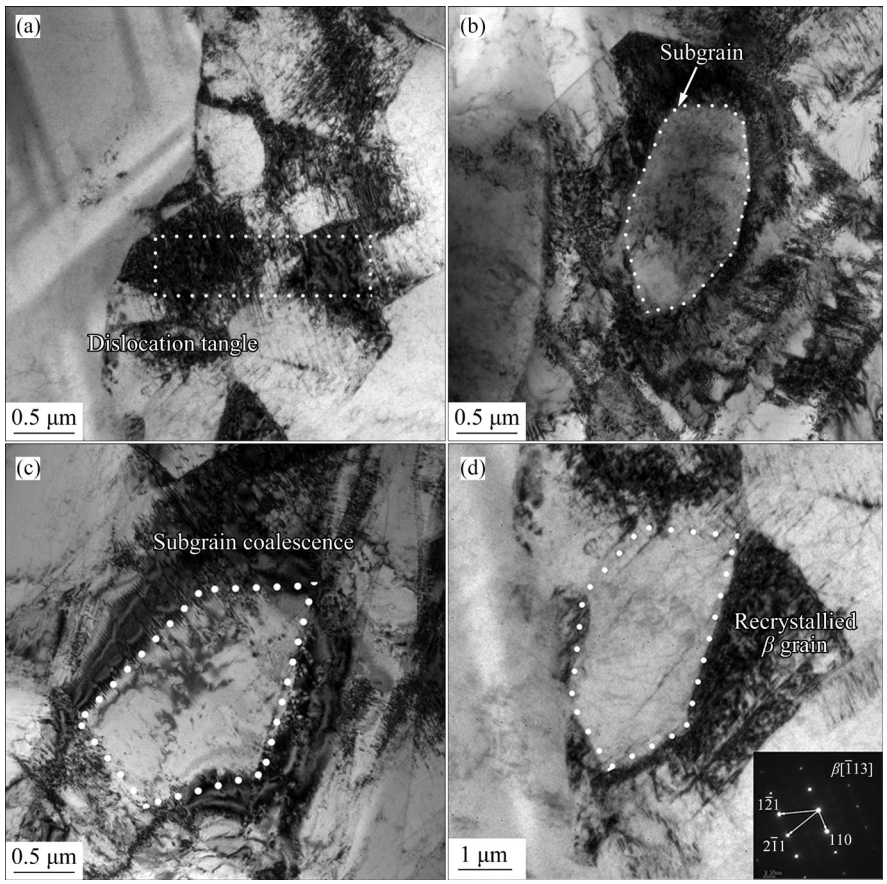

Fig. 9 TEM images of middle area in double-cone specimens deformed at 870 °C: (a) Dislocation tangle; (b) Subgrain; (c) Subgrain coalescence; (d) Recrystallized grain

in the deformed grain. The recrystallized grain formed in the initial grain is shown in Fig. 9(d). The selected area electron diffraction (SAED) was used to calibrate the recrystallized grain. The body-centered cubic structure of the spot calibration indicates that the recrystallized grain is the β grain.

4 Discussion

4.1 Deformation mechanism map

Figure 10 shows the deformation mechanism map of a Ti−5Al−5Mo−5V−1Cr−1Fe titanium alloy. The deformation mechanism map is combined with the homogenization degree of the microstructure under the corresponding deformation conditions. The homogenization degree of the microstructure under different deformation conditions is represented by contour lines. The black contour lines were calculated based on the results of the double-cone compression experiment. The golden contour lines were drawn based on the results of the cylinder compression experiment. The deformation mechanism regions for DRV, DRX, and DBs are

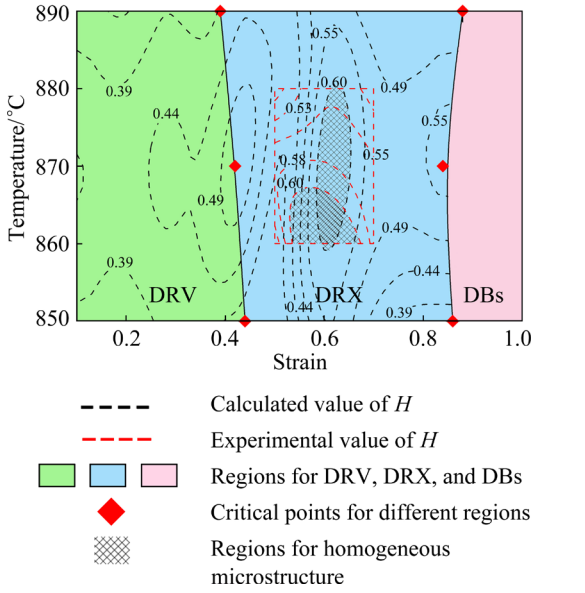

Fig. 10 Deformation mechanism map of Ti−5Al−5Mo−5V−1Cr−1Fe titanium alloy

represented by the regions in green, blue, and purple, respectively. Different deformation mechanism regions are divided by different microstructure morphologies. The minimum strain in the DRX

region is related to the first appearance of polygonal fine grains. The minimal strain in the DBs region is connected to the first appearance of the deformation band.

In the DRV region, the homogenization degree of the microstructure is low under the slight deformation degree. This is because in the early stage of deformation, the DRV only affects a small part of the grains, and most of the grains are not affected. With the increase of strain, the degree of DRV increases, resulting in an increase in homogenization degree of the microstructure. In the DRX region, the microstructure has a higher homogenization degree. The *H* value in the shadow area is higher than 0.6, which indicates that the microstructure under the corresponding deformation condition is homogeneous.

4.2 Dynamic recrystallization and microstructure homogenization

The Ti−5Al−5Mo−5V−1Cr−1Fe titanium alloy has high stacking fault energy (SFE) [24,25]. Due to the high SFE, the width of extended dislocation is narrow, and the climbing and sliding of dislocation are easy to occur [26]. When DRV occurs, the deformation energy stored during the hot deformation is mainly reduced by dislocation annihilation and rearrangement, both of which are completed by the climbing and sliding of dislocation [27]. Therefore, DRV is easy to occur, which results in insufficient dislocation accumulation to prevent discontinuous dynamic recrystallization (DDRX) [28]. As the strain increases, the misorientation of subgrain boundaries gradually increases, and LAGBs gradually transform into HAGBs. This deformation mechanism is called CDRX.

Figure 11 shows the schematic model of the deformation mechanism related to DRV and DRX. The main deformation mechanism is transformed from DRV to DRX as the strain increases. After the start of deformation, a lot of dislocations occur, as shown in Fig. 11(a). Due to the annihilation of redundant dislocations and the rearrangement of the others, the dislocation walls become thinner and clearer, and then transform into LAGBs [29]. Therefore, with the occurrence of DRV, a large number of subgrains and LAGBs appear, as shown in Fig. 11(b).

Figure 11(c) shows the progressive lattice rotation of a part of the subgrains. After the progressive lattice rotation, two adjacent subgrains coalesce, the original subgrain boundary disappears, and LAGBs gradually transform into HAGBs [30]. With the occurrence of DRX, a lot of HAGBs and polygonal grains appear, as shown in Fig. 11(d).

Through the finite element simulation method, the stress−strain curve of Ti−5Al−5Mo−5V−1Cr−1Fe titanium alloy deformed at 870 °C was obtained, as shown in Fig. 12(a).

ZAHIRI et al [31] determined the DRX fraction by processing the stress−strain data. The stress−strain curve and the virtual dynamic recovery curves are shown in Figs. 12(a, b), respectively. The virtual dynamic recovery curve can be extrapolated by the stress−strain curve from the critical strain (ε_c) [32,33]. The DRX fraction (X_{DRX}) is obtained by the following equation [34]:

$$X_{DRX}=\frac{\sigma_{DRV}-\sigma_X}{\sigma_{sat}-\sigma_{ss}} \tag{4}$$

where σ_{DRV} and σ_X represent the flow stresses corresponding to a certain strain on the virtual dynamic recovery curve and the stress−strain curve, respectively; σ_{sat} and σ_{ss} represent the steady-state stresses on the virtual dynamic recovery curve and the stress−strain curve, respectively. The calculation details of the relevant parameters σ_{sat} and ε_c of the virtual dynamic recovery curve are shown in Section B in Supplementary Materials.

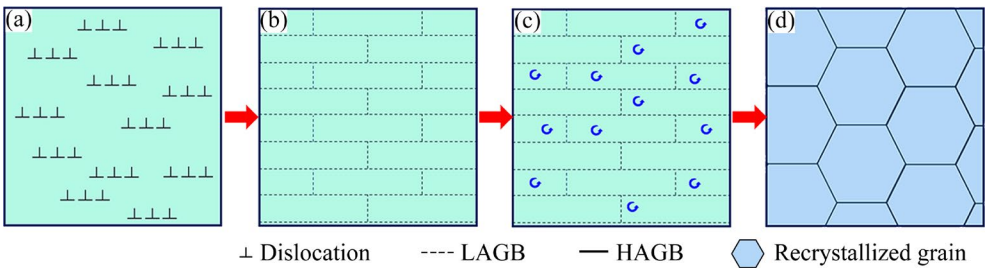

Fig. 11 Schematic model showing deformation mechanism of Ti−5Al−5Mo−5V−1Cr−1Fe titanium alloy

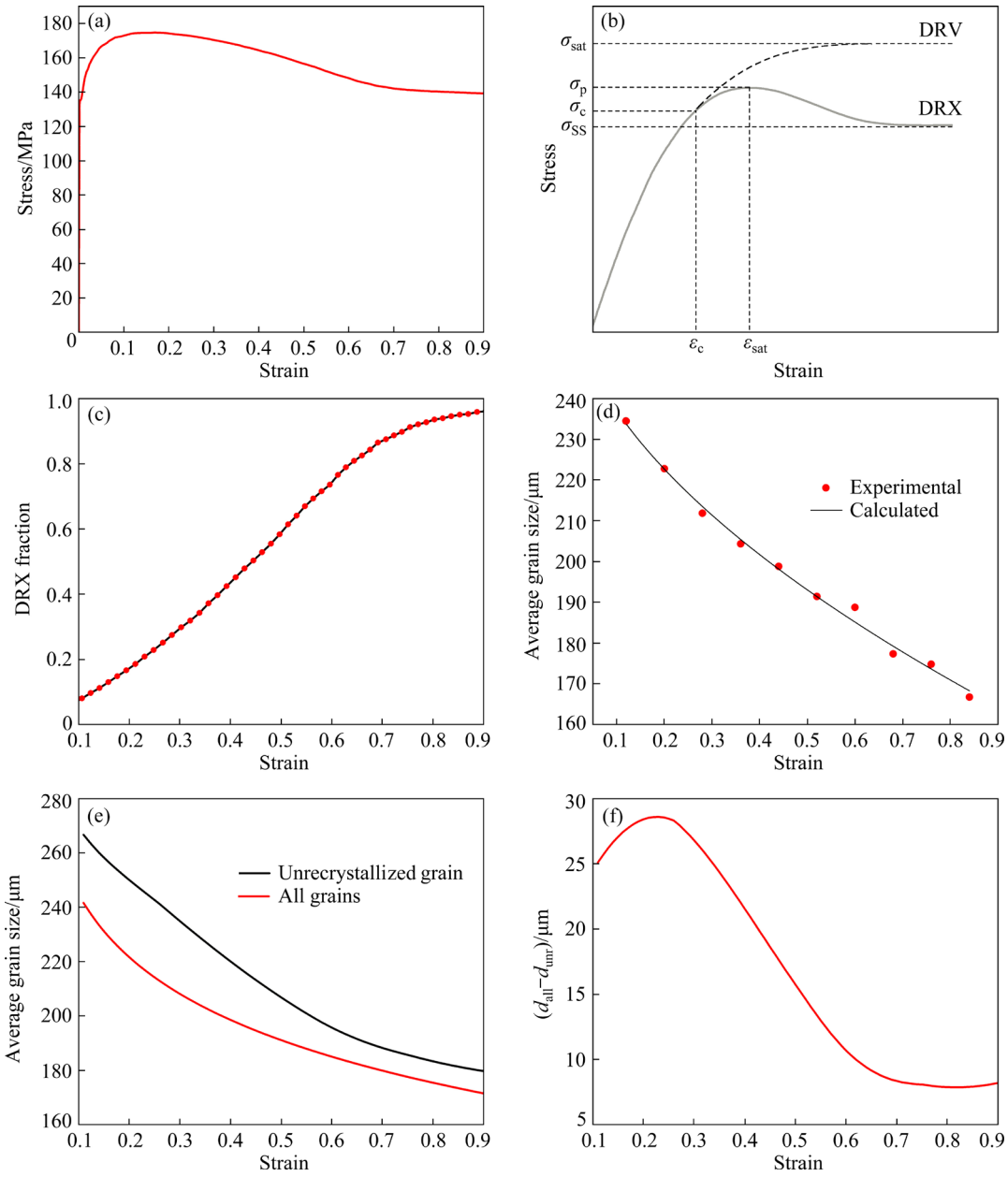

Fig. 12 Calculation of DRX fraction and grain size of Ti−5Al−5Mo−5V−1Cr−1Fe titanium alloy deformed at 870 °C: (a) Strain−stress curve; (b) DRV and DRX curves; (c) DRX fraction; (d, e) Average grain size; (f) Difference between d_{all} and d_{unr}

Figure 12(c) shows the DRX fraction of the Ti−5Al−5Mo−5V−1Cr−1Fe titanium alloy deformed at 870 °C. The deformed microstructure can be divided into recrystallized grains and unrecrystallized grains. The DRX fraction represents the volume fraction of recrystallized grains [32].

The equivalent diameter d_e is used to represent the recrystallization grain size:

$$d_e=\sqrt{d_r \cdot d_z} \tag{5}$$

According to the JMAK model, the average grain size (d_{all}) of titanium alloy after DRX can be expressed by the following equation [35]:

$$d_{all}=ad_0^n\varepsilon^m\dot{\varepsilon}^l \exp[Q/(RT)]+C \tag{6}$$

where d_0 represents the original grain size, and a, n, m and l are material parameters, $\dot{\varepsilon}$ is the strain rate, Q represents the DRX activation energy, which is mainly affected by the temperature, R is the molar gas constant, T is the thermodynamic temperature, and C is a constant.

Figure 12(d) shows the average grain size represented by the equivalent diameter at 870 °C.

By fitting the JMAK equation, the average grain size curve is obtained.

For the recrystallization fraction X_{DRX}, the following equation can be obtained:

$$\frac{\frac{4}{3}\pi\left(\frac{d_{rec}}{2}\right)^3 \cdot n_{rec}}{X_{DRX}} = \frac{\frac{4}{3}\pi\left(\frac{d_{unr}}{2}\right)^3 \cdot n_{unr}}{1-X_{DRX}} \tag{7}$$

where d_{rec} and d_{unr} represent the average grain sizes of the recrystallized grains and the unrecrystallized grains, respectively; n_{rec} and n_{unr} represent the numbers of the recrystallized grains and the unrecrystallized grains, respectively.

In plastic deformation, the volume of the titanium alloy remains unchanged:

$$\frac{4}{3}\pi\left(\frac{d_{rec}}{2}\right)^3 \cdot n_{rec} + \frac{4}{3}\pi\left(\frac{d_{unr}}{2}\right)^3 \cdot n_{unr} = C_1 \tag{8}$$

where C_1 is a constant.

For the average grain size of all grains, the following equation can be obtained:

$$d_{all} = \frac{d_{rec} \cdot n_{rec} + d_{unr} \cdot n_{unr}}{n_{rec} + n_{unr}} \tag{9}$$

According to Eqs. (7), (8), and (9), the average grain size of the unrecrystallized grains d_{unr} is calculated, as shown in Fig. 12(e). Figure 12(f) shows the difference between d_{all} and d_{unr} at 870 °C. The smaller the differential value, the more homogenous the microstructure. As the strain increases from 0.3 to 0.6, the differential value decreases continuously. This shows that DRX can improve the homogenization degree of the microstructure by forming new grains.

5 Conclusions

(1) When the strain is less than 0.42, the deformation mechanism is DRV. In the strain range of 0.42−0.88, the deformation mechanism is DRX. The main deformation mechanism is DBs when the strain exceeds 0.88.

(2) The deformation mechanism map of the Ti−5Al−5Mo−5V−1Cr−1Fe titanium alloy was constructed. The deformation mechanism map is combined with the homogenization degree of the microstructure. The homogeneous deformed microstructure was obtained at the strain of 0.6 and the temperature of 860 °C. The DRX promotes the homogenization degree of the microstructure.

CRediT authorship contribution statement

Yang-zhi-hong XIAO: Conceptualization, Methodology, Formal analysis, Investigation, Data curation, Writing − Original draft, Visualization; **Ye-chen DENG:** Formal analysis, Investigation; **Yi-xin AN** and **Xiao-dong ZHAN:** Formal analysis; **Xiao-yong ZHANG:** Funding acquisition; **Bing-feng WANG:** Conceptualization, Writing − Review & editing, Funding acquisition.

Declaration of competing interest

The authors declare that they have no known competing financial interests or personal relationships that could have appeared to influence the work reported in this paper.

Acknowledgments

The present work was supported by the National Natural Science Foundation of China (Nos. 52441410, 52020105013), and the State Key Laboratory for Powder Metallurgy, China (No. 2022). The authors would like to present their sincere thanks to Ms. Ying MAO at the Central South University for the experimental work.

Supplementary Materials

Supplementary Materials in this paper can be found at: http://tnmsc.csu.edu.cn/download/10-p2568-2023-1266-Supplementary_Materials.pdf.

References

[1] NING Yong-quan, XIE Bing-chao, LIANG Hou-quan, LI He-jun, YANG Xue-mei, GUO Hong-zhen. Dynamic softening behavior of TC18 titanium alloy during hot deformation [J]. Materials & Design, 2015, 71: 68−77.

[2] KANG Li-mei, YANG Chao. A review on high-strength titanium alloys: Microstructure, strengthening, and properties [J]. Advanced Engineering Materials, 2019, 21: 1801359.

[3] BANIA P J. Beta titanium alloys and their role in the titanium industry [J]. JOM, 1994, 46: 16−19.

[4] GHASEMI E, ZAREI-HANZAKI A, FARABI E, TESAŘ K, JÄGER A, REZAEE M. Flow softening and dynamic recrystallization behavior of BT9 titanium alloy: A study using process map development [J]. Journal of Alloys and Compounds, 2017, 695: 1706−1718.

[5] HUANG Liang, LI Chang-min, LI Cheng-lin, HUI Song-xiao, YU Yang, ZHAO Ming-jie, GUO Shi-qi, LI Jian-jun. Research progress on microstructure evolution and hot processing maps of high strength β titanium alloys during hot deformation [J]. Transactions of Nonferrous Metals Society of China, 2022, 32: 3835−3859.

[6] GUPTA A, KHATIRKAR R, SINGH J. A review of microstructure and texture evolution during plastic deformation and heat treatment of β-Ti alloys [J]. Journal of

Alloys and Compounds, 2022, 899: 163242.

[7] LI Hui-zhong, LONG Yu, LIANG Xiao-peng, CHE Yi-xuan, LIU Zhen-qi, LIU Yong, XU Hao, WANG Li. Effects of multiaxial forging on microstructure and high temperature mechanical properties of powder metallurgy Ti−45Al−7Nb−0.3W alloy [J]. Intermetallics, 2020, 116: 106647.

[8] ZHANG Chang-jiang, GUO Chong-xiao, ZHANG Shu-zhi, FENG Hong, CHEN C Y, ZHANG Hong-zhou, CAO Peng. Microstructural manipulation and improved mechanical properties of a near α titanium alloy [J]. Materials Science and Engineering: A, 2020, 771: 138569.

[9] SUÁREZ FERNÁNDEZ D S, WYNNE B P, CRAWFORTH P, FOX K, JACKSON M. The effect of forging texture and machining parameters on the fatigue performance of titanium alloy disc components [J]. International Journal of Fatigue, 2021, 142: 105949.

[10] CHEN Zhao-qi, XU Li-juan, CAO Shou-zhen, YANG Jian-kai, ZHENG Yun-fei, XIAO Shu-long, TIAN Jing, CHEN Yu-yong. Characterization of hot deformation and microstructure evolution of a new metastable β titanium alloy [J]. Transactions of Nonferrous Metals Society of China, 2022, 32: 1513−1529.

[11] LU Tong, DAN Zhen-hua, LI Kai, YI Dan-qing, ZHOU Lian, CHANG Hui. Hot deformation behaviors and dynamic recrystallization mechanism of Ti-35421 alloy in β single field [J]. Transactions of Nonferrous Metals Society of China, 2022, 32: 2889−2907.

[12] SUN Yong-gang, ZHANG Chang-jiang, FENG Hong, ZHANG Shu-zhi, HAN Jian-chao, ZHANG Wang-gang, ZHAO Er-tuan, WANG Hong-wei. Dynamic recrystallization mechanism and improved mechanical properties of a near alpha high temperature titanium alloy processed by severe plastic deformation [J]. Materials Characterization, 2020, 163: 110281.

[13] BOBBILI R, MADHU V. Constitutive modeling of dynamic flow behavior of Ti-5553 alloy [J]. Journal of Alloys and Compounds, 2019, 787: 260−266.

[14] KIM I S, OH J M, LEE S W, YEOM J T, HONG J K, PARK C H, LEE T. Accelerating globularization in additively manufactured Ti−6Al−4V by exploiting martensitic laths [J]. Journal of Materials Research and Technology, 2021, 12: 304−315.

[15] AN Yi-xin, DENG Ye-chen, ZHANG Xiao-yong, WANG Bing-feng. Deformation mechanism diagram of a Ti−2.5Zr−2Al titanium alloy forged in the alpha plus beta region and grain refinement [J]. Materials Science and Engineering A, 2022, 854: 143776.

[16] DENG Ye-chen, AN Yi-xin, XIAO Yang-zhi-hong, ZHAN Xiao-dong, ZHANG Xiao-yong, WANG Bing-feng. Deformation mechanism diagram and deformation instability of a Ti−5Al−5Mo−5V−1Cr−1Fe titanium alloy during the hot compression [J]. Journal of Alloys and Compounds, 2023, 966: 171446.

[17] YU Wen-hao, QIE Xi-wang, ZHAO Wen-zheng, NAN Hai, WU Guo-qing. Effect of structural features on microstructure and properties homogeneity based on quantification and statistical analysis for large-scaled complex titanium alloy castings [J]. International Journal of Metalcasting, 2024, 18: 1535−1546.

[18] ZHAO Deng-chuan, WU Guo-qing. Effects of remelting and refining on the microstructure and properties of particle reinforced magnesium−lithium matrix composites [J]. Materials Science and Engineering: A, 2020, 788: 139607.

[19] ZHANG Jing-qi, XU Xin-yu, XUE Jia-yu, LIU Si-nong, DENG Qing-hua, LI Feng, DING Jie, WANG Hui, CHANG Hui. Hot deformation characteristics and mechanism understanding of Ti−6Al−2Sn−4Zr−6Mo titanium alloy [J]. Journal of Materials Research and Technology, 2022, 20: 2591−2610.

[20] LIAN Qi-hao, ZHANG Chang-jiang, FENG Hong, YANG Zhen-bo, ZHANG Shu-zhi, HAN Jian-chao, WANG Tao, PENG Fan, CAO Peng. Hot deformation temperature and pre-deformation effect on silicide precipitation behavior of (TiB+Y_2O_3)/near α-Ti matrix composite [J]. Transactions of Nonferrous Metals Society of China, 2023, 33: 2660−2671.

[21] PANG Hao-yu, LUO Jiao, LI Cong, LI Miao-quan. The role of beta phase in the morphology evolution of α lamellae in a dual-phase titanium alloy during high temperature compression [J]. Journal of Alloys and Compounds, 2022, 910: 164901.

[22] ZHANG Fang-zhou, WANG Bo, CAO Qing-hua, ZHANG Li, ZHANG Hao-yang. Effect of deformation degree on microstructure and mechanical properties evolution of TiB_w/Ti60 composites during isothermal forging [J]. Transactions of Nonferrous Metals Society of China, 2023, 33: 802−815.

[23] WANG Lei, LI Wei, LUAN Shi-yu, JIN Pei-peng, WANG Jin-hui, REN Qian-long, ZHU Lin. Study on hot deformation behavior of as-cast Ti−5Al−5Mo−5V−1Cr−1Fe titanium alloy in (α+β) phase region [J]. Materials Today Communications, 2023, 35: 105797.

[24] SAKAI T, BELYAKOV A, KAIBYSHEV R, MIURA H, JONAS J J. Dynamic and post-dynamic recrystallization under hot, cold and severe plastic deformation conditions [J]. Progress in Materials Science, 2014, 60: 130−207.

[25] GOURDET S, MONTHEILLET F. A model of continuous dynamic recrystallization [J]. Acta Materialia, 2003, 51: 2685−2699.

[26] LU Tong, DAN Zhen-hua, LI Tian-jing, DAI Guo-qing, SUN Yang-yang, GUO Yan-hua, LI Kai, YI Dan-qing, CHANG Hui, ZHOU Lian. Flow softening and microstructural evolution of near beta titanium alloy Ti-35421 during hot compression deformation in the alpha plus beta region [J]. Journal of Materials Research and Technology, 2022, 19: 2257−2274.

[27] WANG Ke, WU Ming-yu, REN Zhao, ZHANG Yu, XIN Ren-long, LIU Qing. Static globularization and grain morphology evolution of α and β phases during annealing of hot-rolled TC21 titanium alloy [J]. Transactions of Nonferrous Metals Society of China, 2021, 31: 2664−2676.

[28] LU Long-long, ZHANG Yan-min, ZHANG Zao-li, SONG Ke-xing, LI Shan-guang, LI Yan, ZHOU Fei, CAO Qi-gao, FENG Qing, ZHANG Bin-bin. Investigation on microstructure and texture evolution of Ti−6Al−3Nb−2Zr−1Mo alloy during hot deformation [J]. Materials Research Express, 2021, 8: 096520.

[29] LYPCHANSKYI O, SLEBODA T, LUKASZEK-SOLEK A, ZYGULA K, WOJTASZEK M. Application of the strain

compensation model and processing maps for description of hot deformation behavior of metastable β titanium alloy [J]. Materials, 2021, 14(8): 2021.

[30] CHEN S F, LI D Y, ZHANG S H, HAN H N, LEE H W, LEE M G. Modelling continuous dynamic recrystallization of aluminum alloys based on the polycrystal plasticity approach [J]. International Journal of Plasticity, 2020, 131: 102710.

[31] ZAHIRI S H, DAVIES C H J, HODGSON P D. A mechanical approach to quantify dynamic recrystallization in polycrystalline metals [J]. Scripta Materialia, 2005, 52(4): 299−304.

[32] YANAGIDA A, YANAGIMOTO J. A novel approach to determine the kinetics for dynamic recrystallization by using the flow curve [J]. Journal of Materials Processing Technology, 2004, 151: 33−38.

[33] SHI Shuang-xi, LIU Xiu-sheng, ZHANG Xiao-yong, ZHOU Ke-chao. Comparison of flow behaviors of near beta Ti-55511 alloy during hot compression based on SCA and BPANN models [J]. Transactions of Nonferrous Metals Society of China, 2021, 31: 1665−1679.

[34] ZHANG Wen-wei, YANG Qiu-yue, TAN Yuan-biao, MA Min, XIANG Song, ZHAO Fei. Simulation and experimental study of dynamical recrystallization kinetics of TB8 titanium alloys [J]. Materials (Basel), 2020, 13(19): E4429.

[35] IRANI M, LIM S, JOUN M. Experimental and numerical study on the temperature sensitivity of the dynamic recrystallization activation energy and strain rate exponent in the JMAK model [J]. Journal of Materials Research and Technology, 2019, 8: 1616−1627.

近β钛合金在α+β相区的均匀化锻造及变形机制

肖阳志宏[1]，邓晔琛[1]，安益昕[1,2]，詹孝冬[1]，张晓泳[2]，汪冰峰[1,2]

1. 中南大学 材料科学与工程学院，长沙 410083；
2. 中南大学 粉末冶金全国重点实验室，长沙 410083

摘　要：通过双圆锥台压缩实验获得了 Ti−5Al−5Mo−5V−1Cr−1Fe 钛合金在应变范围为 0.1~1 的显微组织。采用 EBSD 和 TEM 技术对其显微组织进行了分析。结果表明：当应变小于 0.42 时，其变形机制为动态回复；当应变为 0.42~0.88 时，其变形机制为动态再结晶；当应变超过 0.88 时，出现变形带。构建了与显微组织均匀程度相关的变形机制图。当应变量为 0.6、变形温度为 860 ℃时，获得了较为均匀的变形组织。这是由于动态再结晶形成了新晶粒，减小了晶粒之间的尺寸差，从而提高了显微组织的均匀程度。

关键词：近β钛合金；热变形机制；动态再结晶；均匀程度；双圆锥台压缩实验

(Edited by Wei-ping CHEN)